## **Edelweiss Applied Science and Technology**

ISSN: 2576-8484 Vol. 9, No. 10, 1052-1066 2025 Publisher: Learning Gate DOI: 10.55214/2576-8484.v9i10.10594 © 2025 by the authors; licensee Learning Gate

# Temperature-controlled growth of ZnO Thin films by spray pyrolysis: Influence on physical properties for photovoltaic applications

Ognanmi Ako<sup>1,2</sup>, ©Mazabalo Baneto<sup>1,2\*</sup>, ©Alphonse Déssoudji Gboglo<sup>1,2</sup>, ©Muthusamy Senthilkumar³, Muthiah Haris³

<sup>1</sup>Centre d'Excellence Régional pour la Maîtrise de l'Electricité (CERME), University of Lomé, 01BP 1515, Lomé, Togo. <sup>2</sup>Laboratory on Solar Energy, Department of Physics, Faculty of Sciences, University of Lomé, 01BP 1515, Lomé, Togo; mazbaneto@gmail.com (M.B.).

<sup>3</sup>School of Arts and Natural Sciences, Joy University, Raja Nagar, Vadakangulam, Near Kanyakumari, Tirunelveli Dist.-627116, Tamil Nadu, India.

**Abstract:** This work investigates the influence of deposition temperature on the structural, morphological, and optical properties of zinc oxide (ZnO) thin films synthesized by spray pyrolysis. Films were deposited at 300 °C, 350 °C, and 400 °C using a 0.3 M zinc acetate precursor solution, followed by annealing at 400 °C for 3 hours. X-ray diffraction revealed that all films are polycrystalline with a hexagonal wurtzite structure, exhibiting a preferred (002) orientation that becomes more pronounced at higher deposition temperatures. Fourier-transform infrared spectroscopy confirmed the presence of characteristic Zn–O vibrations and surface functional groups. Scanning electron microscopy showed uniform and dense film coverage, with a distinct change in morphology from aggregated nanocrystals at 300 °C to microplates and nanograins at 350 °C and 400 °C. UV-visible spectroscopy indicated an increase in optical transmittance with temperature, reaching up to 85% at 400 °C in the visible range. The optical band gap slightly increased with deposition temperature, ranging from 3.26 eV to 3.28 eV. Based on the structural, morphological, and optical properties, 400 °C is identified as the optimal deposition temperature for ZnO thin films, offering enhanced crystallinity, surface quality, and optical transparency essential for improving the performance of photovoltaic devices.

Keywords: Deposition temperature, Photovoltaic, Physical properties, Spray pyrolysis, Thin films, Zinc oxide.

# 1. Introduction

Zinc oxide (ZnO) is a transparent conductive oxide belonging to the family of II-VI binary semiconductors [1]. Over the past few years, it has attracted increasing research interest due to its remarkable optoelectronic properties. It exhibits a wide direct bandgap (3.37 eV at 300 K), providing excellent transparency in the visible range [2] as well as a high exciton binding energy (60 meV) [3] and significant electron mobility (205 cm²V-¹s-¹) [4]. In addition, its non-toxicity and natural abundance [5, 6] make it an attractive and sustainable material. Thanks to this combination of properties, ZnO is considered a material of choice and a promising candidate for various applications, including display screens [7], gas sensors [8], laser diodes [9] and photovoltaic cells [10]. In solar cells, particularly in organic solar cells (OSCs), ZnO thin films are commonly used as electron transport layers (ETLs) [11] where their role is to extract and transport charges while ensuring high optical transparency to maximize light harvesting [12]. For this purpose, the films must combine enhanced crystallinity, smooth surface morphology, and high transmittance in the visible range, as these properties directly influence charge mobility, recombination processes, and overall device efficiency [13]. Previous studies

have shown that nanostructured ZnO thin films can meet these requirements [14]. However, the properties of ZnO thin films strongly depend on the deposition techniques employed. ZnO can be synthesized using various methods, including spin coating [15, 16], dip coating [17, 18], chemical bath deposition [19], hydrothermal synthesis [20-22], vacuum thermal evaporation [23-25] and spray pyrolysis [26, 27]. Among these methods, spray pyrolysis is particularly advantageous: it is low-cost, does not require high vacuum or energy-intensive equipment, allows the simultaneous synthesis of multiple samples, and provides good control over the chemical composition of the material [6, 28]. The process involves atomizing a precursor solution onto a substrate heated at a controlled temperature [29, 30]. The quality and properties of thin films prepared by spray pyrolysis are highly dependent on deposition parameters, such as solution concentration, solvent type, nozzle-to-substrate distance, spray flux density, deposition time, dopant concentration, post-deposition annealing, and substrate temperature [31]. Among these parameters, the deposition temperature is particularly critical, as it directly influences the crystalline growth, morphology, and optical properties of ZnO [32]. Previous studies have reported that temperature can significantly influence ZnO properties, but the results remain partially divergent. For instance, Bedia, et al. [32] observed improved transparency with increasing temperature, whereas Bettayeb et al. [33] reported a reduction in transmittance at higher deposition temperatures due to surface roughening. Ouhaibi et al. [34] highlighted notable changes in grain shape and size, while Nezzari et al. [35] demonstrated that higher deposition temperatures promote crystallite growth and a slight widening of the band gap. Although these works confirm the critical role of deposition temperature, the optimal conditions for obtaining ZnO thin films with the combination of structural, morphological, and optical properties required for photovoltaic applications have not yet been clearly defined. The precursor concentration also plays a decisive role in crystalline growth and film quality. In our previous work [26], it was shown that a zinc acetate concentration of 0.3 M represents an optimal condition for obtaining well-crystallized ZnO thin films by spray pyrolysis. Building on this result, the present study focuses exclusively on the role of deposition temperature. ZnO thin films were deposited at 300, 350, and 400 °C using a fixed 0.3 M precursor concentration in order to determine how the structural, morphological, and optical properties evolve, and to identify the deposition temperature that provides the best balance of crystallinity, morphology, and optical transparency for photovoltaic applications.

#### 2. Experimental Details and Characterization

#### 2.1. Reagents

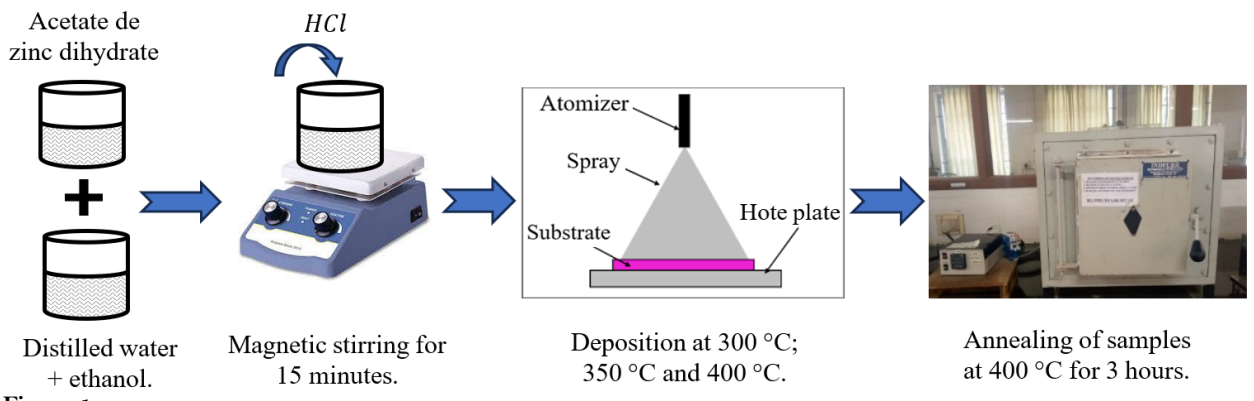
Microscope glass slides were used as substrates for ZnO thin film deposition. Zinc acetate dihydrate  $(CH_3COO)_2Zn$ ,  $2H_2O$ ) (Sigma-Aldrich), ethanol  $(C_2H_6O)$ , acetone  $[(CH_3)_2CO]$ , Nitric acid, nitric acid, and distilled water, all analytical grade (> 99% purity), were employed without further purification. A 2:3 (v/v) distilled water-ethanol mixture was chosen as the solvent due to its low surface tension and viscosity [36] which favors fine droplet formation and uniform substrate coverage, while its high volatility helps minimize substrate cooling during deposition.

#### 2.2. Substrate Cleaning

Glass substrates ( $2.5 \text{ cm} \times 2.0 \text{ cm}$ ) were first immersed for a few minutes in an aqueous nitric acid solution to remove dust and surface impurities. After rinsing with distilled water, the substrates were sequentially cleaned in an ultrasonic bath with acetone, ethanol, and distilled water for 15 minutes each to eliminate all organic and inorganic contaminants. Finally, the substrates were dried under a stream of hot air using a conventional heat blower.

#### 2.3. Formation of ZnO Nanostructured Thin Films

ZnO thin films were deposited on glass substrates at different temperatures, specifically 300°C, 350°C, and 400°C, using the spray pyrolysis technique (HOLMARC, HO-TH-64) to study the effect of substrate temperature on the physical properties of ZnO thin films. Fig. 1 shows the procedure for preparing ZnO thin films. In the spray pyrolysis process, the main sources of Zn used to develop ZnO thin films are zinc chloride, zinc nitrate, zinc acetate, and zinc acetylacetonate [28, 37]. In this work, zinc acetate is used as the zinc precursor, as our previous work has shown that it provides good physical properties [26]. To prepare a 0.3 M solution, a specific mass of zinc acetate was dissolved in distilled water and ethanol in a 2:3 volume ratio to obtain a total volume of 20 mL. A few drops of hydrochloric acid were added to dissolve the zinc hydroxide precipitate. After 15 minutes of magnetic stirring, the solution became clear and ready for deposition using the spray pyrolysis setup. After deposition, all samples were annealed at 400 °C for 3 hours to promote good crystallization.



Experimental procedure for ZnO thin film deposition via spray pyrolysis.

#### 2.4. Characterization of ZnO Nanostructured Thin Films

The properties of ZnO thin films were analyzed using several complementary techniques. X-ray diffraction (EMPYREAN,  $\lambda = 1.5406$  Å, Cu-K $\alpha$ ) was employed to determine the crystalline structure and phase composition. Surface morphology was examined by scanning electron microscopy (ZEISS-EVO 18, 15 kV). Functional groups and chemical bonds were characterized by Fourier-transform infrared spectroscopy (Perkin-Elmer Spectrum 3, 4000 - 400 cm<sup>-1</sup> in GladiATR mode). The optical transmittance of the thin films was measured using UV-visible spectrophotometry (JASCO V-670).

## 3. Results and Discussion

#### 3.1. Structural Properties

Figure 2 shows the X-ray diffraction (XRD) patterns of ZnO thin films deposited at temperatures ranging from 300 °C to 400 °C. For all samples, the diffraction peaks match those of JCPDS card No. 36-1451, corresponding to the wurtzite phase of ZnO with a hexagonal structure and space group P63mc [38]. The XRD results indicate that deposition temperature significantly influences the film's crystallographic orientation. At 300 °C, the films exhibit randomly oriented crystallites. However, starting from 350 °C, a pronounced preferential orientation along the (002) plane emerges, indicating that the crystallites tend to align with their c-axis perpendicular to the substrate surface. This evolution is attributed to the increase in kinetic energy of ZnO atoms with temperature, which promotes atomic migration toward low-energy crystallographic planes [39]. At lower temperatures, such as 300 °C, the

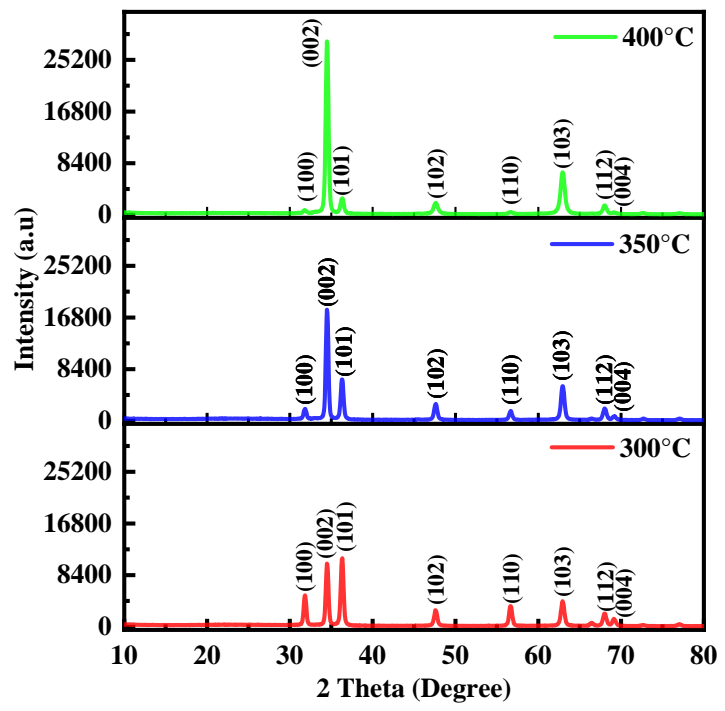
atoms possess insufficient energy to reach energetically favorable positions, resulting in less ordered growth [40].

Furthermore, when using the spray pyrolysis technique, ZnO tends to grow predominantly along the (002) orientation due to the low surface free energy of the (002) plane [41]. To confirm the degree of preferential orientation of the crystallites along the (002) axis, the texture coefficient  $T_{C(hkl)}$  for each was calculated using equation (1):

$$T_{C(hkl)} = \frac{\left[\frac{I_{(hkl)}}{I_{r(hkl)}}\right]}{\frac{1}{n}\left[\sum_{n}\left(\frac{I_{(hkl)}}{I_{r(hkl)}}\right)\right]}$$
(1)

where  $T_{C(hkl)}$  is the texture coefficient,  $I_{(hkl)}$  represents the XRD intensities obtained from the thin films, and n is the number of diffraction peaks considered  $I_{r(hkl)}$  is the reference XRD intensity (JCPDS card No. 36-1451) for randomly oriented grains.

The  $T_{C(hkl)}$  values calculated for the (100), (002), and (101) planes as a function of deposition temperature are summarized in Table 1. A marked increase in the  $T_{C(002)}$  plane is observed, rising from 1.613 at 300 °C to 2.820 at 400 °C. At the lower temperature of 300 °C, the  $T_{C(002)}$  values for the different planes are relatively close to one another, indicating a nearly random orientation of crystallites. This behavior can be attributed to limited atomic mobility at lower temperatures, which hinders the rearrangement of atoms into energetically favorable orientations [42]. In contrast, at higher deposition temperatures (350 °C and 400 °C), the (002) orientation becomes dominant, with  $T_C$  values increasing to 2.407 and 2.820, respectively, indicate a strong preferential growth along the c-axis, perpendicular to the substrate surface. This is typically associated with improved crystallinity and film quality. The correspondingly low  $T_C$  values for the (100) and (101) planes further support the preferential alignment along the (002) direction. These results are consistent with the XRD patterns, confirming the temperature-dependent evolution of ZnO thin film texture.



XRD patterns of ZnO thin films deposited at different temperatures.

The lattice parameters a and c, as well as the interplanar spacing  $d_{hkl}$  of the hexagonal wurtzite structure of all the synthesized ZnO thin films was calculated using relations (2-4) [43] and are presented in Table 1.

$$a^{2} = \frac{\lambda^{2} (A_{1}B_{2} - A_{2}B_{1})}{3(B_{2}\sin^{2}\theta_{1} - B_{1}\sin^{2}\theta_{2})}$$
(2)

$$c^{2} = \frac{\lambda^{2} (A_{1}B_{2} - A_{2}B_{1})}{4(A_{1}\sin^{2}\theta_{2} - A_{2}\sin^{2}\theta_{1})}$$
(3)

$$a^{2} = \frac{\lambda^{2} (A_{1}B_{2} - A_{2}B_{1})}{3(B_{2}\sin^{2}\theta_{1} - B_{1}\sin^{2}\theta_{2})}$$

$$c^{2} = \frac{\lambda^{2} (A_{1}B_{2} - A_{2}B_{1})}{4(A_{1}\sin^{2}\theta_{2} - A_{2}\sin^{2}\theta_{1})}$$

$$\frac{1}{d_{hkl}^{2}} = \frac{4}{3} \left(\frac{h^{2} + hk + k^{2}}{a^{2}}\right) + \frac{l^{2}}{c^{2}}$$
(4)

where  $\lambda$  is the wavelength of the X-rays (1.540 Å),  $\theta$  is the diffraction angle, h, k, l are the Miller indices,  $d_{hkl}$  is the interplanar spacing, and the coefficients A<sub>1</sub>, A<sub>2</sub>, B<sub>1</sub>, and B<sub>2</sub> are determined for a pair of planes  $(h_1k_1k_1)$  and  $(h_2k_2l_2)$  corresponding respectively to the angles  $\theta_1$  and  $\theta_2$ , such that: que  $\begin{cases} A_1=h_1^2+h_1k_1+k_1^2 \\ A_2=h_2^2+h_2k_2+k_2^2 \end{cases}$ ,  $\begin{cases} B_1=l_1^2 \\ B_2=l_2^2 \end{cases}$ 

As shown in Table 1, the calculated lattice parameters a and c for the ZnO thin films are in close agreement with the standard reference values (a = 3.249 Å and c = 5.206 Å) reported in JCPDS card no. 36-1451 [38]. No significant variation in these parameters is observed with changes in deposition temperature, indicating that the hexagonal wurtzite structure is maintained across all samples. The c/a ratio remains approximately 1.602 for all films, further confirming the formation of a well-ordered hexagonal lattice. Similarly, the interplanar spacing values ( $d_{hkl}$ ), show negligible variation with deposition temperature. For all investigated conditions (300 °C, 350 °C, and 400 °C), the (002) interplanar spacing remains constant at approximately d = 2.599 Å, which is very close to the standard value of 2.603 Å. The slight reduction compared to the theoretical value may be attributed to internal stresses or strain effects within the crystal lattice, possibly induced during film growth or post-deposition annealing [44].

Table 1.

Lattice parameters and structural properties of ZnO thin films derived from the (002) diffraction peak, deposited at different temperatures.

Temperatures (°C)	<b>2</b> θ(°)	β (°)	D(nm)	d(Å)	$\frac{\delta \left(\times 10^{14}\right.}{\text{lines/m}^2\right)}$	Lattice parameters			L(Å)	<i>V</i> (Å <sup>3</sup> )	$T_{\mathcal{C}(hkl)}$		
						a (Å)	c(Å)	c/a	D(M)	V(A)	(100)	(002)	(101)
300	34.486	0.386	21.530	2.599	2.157	3.241	5.202	1.605	1.974	47.317	0.618	1.613	0.769
350	34.486	0.369	22.512	2.599	1.973	3.249	5.191	1.598	1.976	47.448	0.200	2.407	0.394
400	34.486	0.400	20.772	2.599	2.318	3.239	5.215	1.610	1.974	47.370	0.062	2.820	0.118
JCPDS N°31-1451	34.422	-	-	2.603	-	3.250	5.207	1.602	-	47.622	-	-	-

Edelweiss Applied Science and Technology

ISSN: 2576-8484

Vol. 9, No. 10: 1052-1066, 2025

DOI: 10.55214/2576-8484.v9i10.10594 © 2025 by the authors; licensee Learning Gate The influence of temperature on crystallite size, bond length, unit cell volume, and dislocation density was studied. To this end, the crystallite size (D) was calculated using the Debye-Scherrer formula (Equation 5) [45]:

$$D = \frac{0.9\lambda}{\beta \cos\theta} \tag{5}$$

where k is a constant taken as 0.9,  $\lambda$  is the wavelength of the X-ray source used (1.540 Å),  $\beta$  is the full width at half maximum (FWHM) of the peak, and  $\theta$  is the Bragg diffraction angle. The FWHM of the (002) diffraction peak exhibits a slight decrease from 0.386° at 300 °C to 0.369° at 350 °C, indicating an improvement in crystallinity. The corresponding crystallite sizes, calculated using the Debye-Scherrer equation, increase from 21.53 nm to 22.51 nm. This enhancement is likely due to increased thermal energy at 350 °C, which facilitates atomic mobility and promotes better structural organization [42]. However, at 400 °C, the FWHM increases to 0.400°, suggesting a reduction in crystallite size to 20.77 nm. This decrease may be attributed to structural rearrangements or the generation of additional defects caused by excessive thermal energy during deposition [42]. Such effects can disrupt long-range order and reduce average crystallite dimensions, despite the higher substrate temperature.

The dislocation density ( $\delta$ ), which represents the number of defects resulting from internal deformation and the mismatch between the substrate and crystal growth, was calculated according to equation (6) [31]:

$$\delta = \frac{1}{D^2} \tag{6}$$

where D is the crystallite size. A low dislocation density reflects a more structurally perfect crystal with fewer defects, which is essential for enhancing the electronic and optical properties of ZnO thin films. At a deposition temperature of 300 °C, the dislocation density is relatively high (2.157×10<sup>14</sup> lines/m²), indicating a significant number of crystal imperfections. This elevated defect density is consistent with the small crystal size (21.53 nm) and disordered grain growth observed at this temperature. As the deposition temperature increases to 350 °C, the dislocation density decreases markedly to 1.973×10<sup>14</sup> lines/m². This reduction corresponds with an increase in crystallite size (22.51 nm), reflecting improved crystalline quality. The enhanced atomic mobility at this temperature promotes grain coalescence and the reduction of structural defects, leading to better film organization and fewer dislocations [46]. However, at 400°C, the dislocation density increases again to 2.318×10<sup>14</sup> lines/m², despite a strong preferential orientation along (002). This increase may result from rapid recrystallization, sub-grain formation, or internal stresses induced by local overheating [47]. Such phenomena can fragment crystallites or introduce new defects, thereby compromising structural uniformity. These results suggest the existence of an optimal deposition temperature, here identified as 350 °C, above which excessive thermal energy begins to degrade the crystalline integrity of the ZnO films

The volume of the hexagonal cell (v) was evaluated by equation (7) [48]:

$$v = \left(\frac{\sqrt{3}}{2}\right)a^2c\tag{7}$$

The unit cell volume of ZnO thin films shows a slight variation with deposition temperature, increasing from 47.317 ų at 300 °C to a maximum of 47.448 ų at 350 °C, before decreasing slightly to 47.370 ų at 400 °C. The highest volume observed at 350 °C coincides with the temperature at which the crystallite size is maximized and the (002) preferential orientation is most pronounced. This suggests that the crystal growth at this temperature is more ordered and experiences fewer internal strains.

The bond length of ZnO is calculated by equation (8) [49]:

$$L = \sqrt{\frac{a^2}{3} + \left(\frac{1}{2} - u\right)^2 \cdot c^2} \tag{8}$$

where u is a parameter related to the c/a ratio, and u is a measure of the amount of each atom displaced relative to the next along the c axis, and is given by the following formula (9) \[ 50 \]:

$$u = \frac{a^2}{3c^2} + 0.25\tag{9}$$

The Zn-O bond length also exhibits minimal variation with temperature, ranging from 1.974 Å to 1.976 Å. This stability indicates that the local atomic arrangement remains largely unaffected by thermal fluctuations, reflecting the robustness of the Zn-O chemical bonding within the wurtzite lattice.

### 3.2. Morphological Properties

Figure 2 shows SEM images of thin films deposited at 300 °C, 350 °C, and 400 °C. The films deposited at 350 °C and 400 °C exhibit dense, homogeneous, and smooth surfaces, whereas the film obtained at 300 °C appears more porous, with a less compact morphology. At 300 °C, the surface is characterized by aggregates and grains composed of small crystals, along with the presence of irregularly shaped microplates. These microstructures tend to diminish with increasing temperature, indicating a thermally driven morphological evolution. This change is attributed to temperaturedependent growth mechanisms [39]. At 300 °C, the precursor droplets reach the substrate, where solvent evaporation and only partial decomposition of zinc acetate occur. This incomplete decomposition at this temperature, despite the known decomposition onset of zinc acetate around 180-200 °C, may explain the possible residual presence of organic species, although no secondary phases were detected in XRD, likely due to their low concentration. In contrast, at 400 °C, solvent evaporation occurs before the droplets reach the substrate, enabling more complete precursor decomposition [42]. The enhanced thermal energy at higher temperatures also promotes grain coalescence, leading to the formation of larger, well-defined aggregates and a more compact film structure. Notably, the grains formed at 350°C become larger at 400°C, indicating an agglomeration effect favored by increased atomic mobility and surface diffusion [42]. These morphological observations are in good agreement with XRD results.

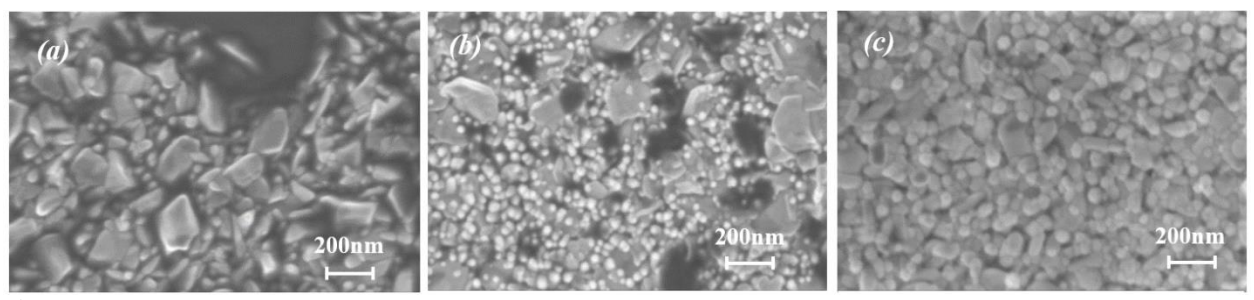


Figure 1.

SEM images of ZnO thin films deposited at different temperatures (a) 300 °C, (b) 350 °C and (c) 400 °C.

#### 3.3. Optical Properties

Figure 4 shows the optical transmission spectra of ZnO thin films deposited at different temperatures. Measurements were performed in the UV-visible range (400 - 900 nm). In this spectral region, pronounced interference fringes are observed, originating from multiple reflections at the film

surface and the film/substrate interface, as well as from light scattering, which is more pronounced for small grain sizes. The presence of such fringes also indicates a relatively smooth surface and a uniform film, which is consistent with the SEM observations at higher deposition temperatures.

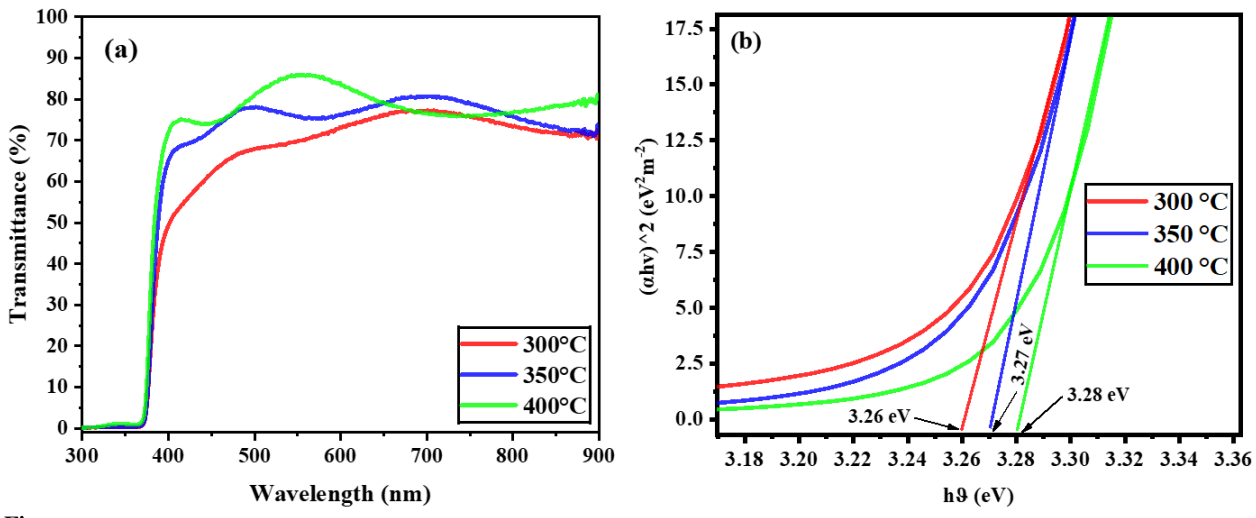


Figure 4.
(a) Optical transmittance spectra of ZnO thin films deposited at different temperatures and (b) Tauc's plot of ZnO thin films for different temperatures.

All deposited films exhibit good transmittance (≥ 75%) in the visible region, with a decrease in transmittance observed between 300 and 400 nm, corresponding to the fundamental absorption edge of ZnO related to electronic bandgap transitions. In the visible range (400-700 nm), optical transmittance increases significantly with deposition temperature, rising from approximately 75% at 300 °C to 80% at 350 °C, and reaching about 85% at 400 °C. This improvement at higher temperatures is attributed to enhanced crystallinity and reduced defect density, as confirmed by XRD analysis, which showed narrower diffraction peaks and a stronger preferential orientation along the (002) plane. A better crystalline structure minimizes grain boundary scattering and defect-related absorption, thereby allowing more efficient light transmission through the films. Furthermore, SEM micrographs revealed a denser and more compact microstructure at higher deposition temperatures, which also contributes to reduced diffuse scattering. These combined effects improved crystal ordering, reduced internal stresses, and smoother, more compact surface morphology, result in superior optical transparency. Such high transmittance, particularly at 400 °C, is advantageous for photovoltaic applications, where maximizing light entry into the active layer is critical for device efficiency.

The optical band gap energy (Eg) was estimated from the absorption spectra by analyzing the variation of the absorption coefficient ( $\alpha$ ) as a function of photon energy, in accordance with Tauc's relation [51]:

$$(\alpha h \vartheta)^n = A(h \vartheta - E_g) \tag{10}$$

where  $\alpha$ , n, Eg, and  $h\vartheta$  are the absorption coefficient, power factor of the transition mode, band-gap energy, and photon energy, respectively. Fig 4.b shows the plots of  $(\alpha h\vartheta)^2$  versus  $(h\vartheta)$  for the ZnO samples deposited at 300, 350, and 400 °C. Extrapolating the linear portion of each curve to the energy axis yielded Eg values of 3.26, 3.27, and 3.28 eV, respectively. This slight increase in Eg with deposition temperature can be attributed to the reduction of structural disorder and defect density within the films  $\lceil 32 \rceil$  as suggested by the XRD results showing improved crystallinity, a lower defect concentration

limits the formation of localized states within the band gap, thus sharpening the absorption edge and shifting it towards higher energies. Such behavior is consistent with reports in the literature [32] where improved atomic ordering at higher temperatures leads to a widening of the optical band gap. Furthermore, the combination of high transparency (up to 85% in the visible range) and a suitable band gap close to 3.28 eV makes the film deposited at 400°C particularly promising for use as an electron transport layer in photovoltaic devices.

### 3.4. FTIR Analysis

Figure 5 shows the FT-IR spectra of ZnO thin films deposited on glass substrates at different temperatures. The results indicate that the deposition temperature does not significantly affect the functional groups or chemical bonds present in the films. In the range of 3500 - 4000 cm<sup>-1</sup>, peaks characteristic of O-H vibrations are observed, independent of the deposition temperature. These may originate from the ethanol used as the solvent [52]. All samples also exhibit absorption bands at 2919 and 760 cm<sup>-1</sup>, corresponding to the C-H stretching vibrations of alkane groups [53] likely derived from zinc acetate dihydrate. Peaks around 2150 cm<sup>-1</sup> are associated with the O=C=O stretching mode of carbon dioxide, while a band at 1590 cm<sup>-1</sup> is attributed to symmetric C=O stretching [54]. Signals between 700 and 1200 cm<sup>-1</sup> correspond to H-O-H bending vibrations, due to the presence of crystallization water from the solvent [55]. The band at 883 cm<sup>-1</sup> is also related to water deformation vibrations. Finally, the region around 460 cm<sup>-1</sup>, present in all samples, is characteristic of Zn-O vibrations, in agreement with previous studies [56].

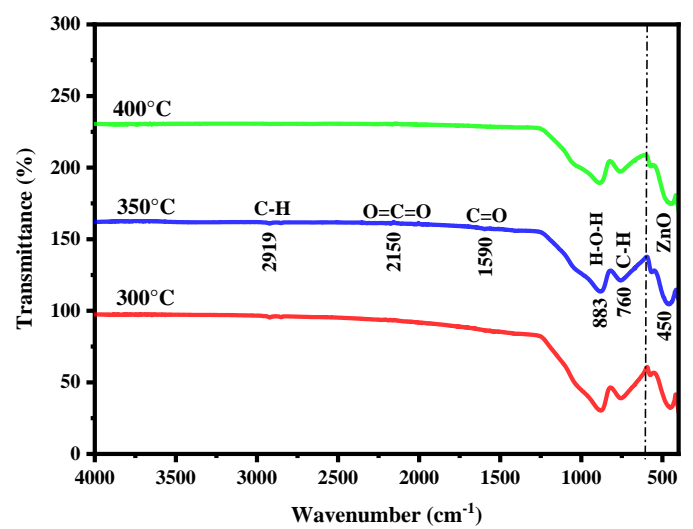


Figure 5.
FTIR spectra of ZnO thin films deposited at different temperatures.

#### 4. Conclusion

ZnO thin films were deposited on glass substrates at 300 °C, 350 °C, and 400 °C using spray pyrolysis methods. The effect of temperature on the physical properties was studied. X-ray diffraction analysis showed that all films crystallize in the hexagonal wurtzite phase, with increasing preferential orientation along the (002) plane as the deposition temperature rises, due to enhanced atomic mobility. SEM images revealed that films grown at 350 °C and 400 °C are dense, uniform, and smooth, whereas those deposited at 300 °C exhibited a porous morphology with grain aggregates. Optical transmission in the visible region improved with increasing temperature, reaching a maximum transmittance of 85% at

400 °C, which is attributed to better crystallinity and reduced structural defects. The bandgap energy increased with deposition temperature, measuring 3.26 eV, 3.27 eV, and 3.28 eV for films deposited at 300, 350, and 400 °C, respectively. FT-IR analysis confirmed the presence of characteristic Zn–O bond vibrations in all samples. Considering the structural, morphological, and optical properties, 400 °C is identified as the optimal deposition temperature for ZnO thin films intended for photovoltaic applications, providing enhanced crystallinity, surface quality, and optical transparency essential for device performance.

## **Funding:**

This research work received financial support from Centre d'Excellence Régional pour la Maîtrise de l'Electricité (CERME) of the University of Lomé (crédit IDA 6512-TG, Don IDA 536IDA).

## Transparency:

The authors confirm that the manuscript is an honest, accurate, and transparent account of the study; that no vital features of the study have been omitted; and that any discrepancies from the study as planned have been explained. This study followed all ethical practices during writing.

## **Acknowledgements:**

The authors would like to thank FICCI-DST (Government of India) for their support through the CV Raman International Fellowship Program for African Researchers.

# **Copyright:**

© 2025 by the authors. This article is an open access article distributed under the terms and conditions of the Creative Commons Attribution (CC BY) license (<a href="https://creativecommons.org/licenses/by/4.0/">https://creativecommons.org/licenses/by/4.0/</a>).

## References

- [17] B. Krishnan et al., Group II–VI semiconductors. Cham: Springer, 2019.
- M. Younas and K. Harrabi, "Performance enhancement of dye-sensitized solar cells via co-sensitization of ruthenium (II) based N749 dye and organic sensitizer RK1," *Solar Energy*, vol. 203, pp. 260-266, 2020. https://doi.org/10.1016/j.solener.2020.04.051
- Q. Zhang, C. S. Dandeneau, X. Zhou, and G. Cao, "ZnO nanostructures for dye-sensitized solar cells," *Advanced Materials*, vol. 21, no. 41, pp. 4087-4108, 2009. https://doi.org/10.1002/adma.200803827
- [4] A. K. Ambedkar *et al.*, "Structural, optical and thermoelectric properties of Al-doped ZnO thin films prepared by spray pyrolysis," *Surfaces and Interfaces*, vol. 19, p. 100504, 2020. https://doi.org/10.1016/j.surfin.2020.100504
- A. Hafdallah, F. Ynineb, W. Daranfed, N. Attaf, and M. S. Aida, "Structural, optical and electrical properties of ZnO:Al thin films produced by ultrasonic spray," *Revue Nature et Technologie*, vol. 4, no. 1, pp. 25-27, 2012.
- [6] K. Dakhsi, B. Hartiti, S. Elfarrass, H. Tchognia, M. E. Touhami, and P. Thevenin, "Study of the structural, optical and electrical properties of Al-doped ZnO thin films deposited by spray pyrolysis," *Afrique Science: Revue Internationale des Sciences et Technologie*, vol. 10, no. 3, 2014.
- [7] F. T. Z. Toma, M. S. Rahman, and K. H. Maria, "A review of recent advances in ZnO nanostructured thin films by various deposition techniques," *Discover Materials*, vol. 5, no. 1, p. 60, 2025. https://doi.org/10.1007/s43939-025-00201-1
- [8] S. Agarwal et al., "Gas sensing properties of ZnO nanostructures (flowers/rods) synthesized by hydrothermal method," Sensors and Actuators B: Chemical, vol. 292, pp. 24-31, 2019. https://doi.org/10.1016/j.snb.2019.04.083
- [9] N. S. Davamani, J. Mariadhas, P. M. D. Samuel, and S. R. I. Savariroyan, "The effect of Mg doping on structural and catalytic removal of malachite green using ZnO thin films fabrication by cost effective home-made spray pyrolysis technique," *Next Materials*, vol. 8, p. 100884, 2025. https://doi.org/10.1016/j.nxmate.2025.100884
- [10] A. Djelloul, K. Bouzid, and F. Guerrab, "Role of substrate temperature on the structural and morphological properties of ZnO thin films deposited by ultrasonic spray pyrolysis," *Turkish Journal of Physics*, vol. 32, no. 1, pp. 49-58, 2008.

- [11] Y. Lare et al., "Effect of a zinc oxide, at the cathode interface, on the efficiency of inverted organic photovoltaic cells based on the CuPc/C60 couple," Journal of Materials Science: Materials in Electronics, vol. 22, no. 4, pp. 365-370, 2011. https://doi.org/10.1007/s10854-010-0143-6
- D. Hatem, F. Nemmar, and M. S. Belkaid, "Organic solar cells: Material selection, device structures, and improved efficiency and stability," *Journal of Renewable Energies*, vol. 12, no. 1, pp. 77-86, 2009. https://doi.org/10.54966/jreen.v12i1.121
- [13] M. Baneto, A. Enesca, Y. Lare, K. Jondo, K. Napo, and A. Duta, "Effect of precursor concentration on structural, morphological and opto-electric properties of ZnO thin films prepared by spray pyrolysis," *Ceramics International*, vol. 40, no. 6, pp. 8397-8404, 2014. https://doi.org/10.1016/j.ceramint.2014.01.048
- [14] A. Kołodziejczak-Radzimska and T. Jesionowski, "Zinc oxide—from synthesis to application: A reviewa," *Materials*, vol. 7, no. 4, pp. 2833-2881, 2014. https://doi.org/10.3390/ma7042833
- [15] S. Ilican, Y. Caglar, and M. Caglar, "Preparation and characterization of ZnO thin films deposited by sol-gel spin coating method," *Journal of Optoelectronics and Advanced Materials*, vol. 10, no. 10, pp. 2578-2583, 2008.
- D. A. Ajadi, S. M. Agboola, and O. Adedokun, "Effect of spin coating speed on some optical properties of ZnO thin films," *Journal of Materials Science and Chemical Engineering*, vol. 4, no. 5, pp. 1-6, 2016. https://doi.org/10.4236/msce.2016.45001
- [17] K. L. Foo, U. Hashim, K. Muhammad, and C. H. Voon, "Sol-gel synthesized zinc oxide nanorods and their structural and optical investigation for optoelectronic application," *Nanoscale Research Letters*, vol. 9, no. 1, p. 429, 2014. https://doi.org/10.1186/1556-276X-9-429
- [18] N. M. Arifin, E. E. Mhd Noor, F. Mohamad, and N. Mohamad, "The impact of spinning speed on n-tio2/zno bilayer thin film fabricated through sol-gel spin-coating method," *Coatings*, vol. 14, no. 1, p. 73, 2024. https://doi.org/10.3390/coatings14010073
- [19] A. D. Gboglo *et al.*, "Co-effect of ph control agent and ph value on the physical properties of zno thin films obtained by chemical bath deposition for potential application in dye-sensitized solar cells," *Surfaces*, vol. 8, no. 3, p. 46, 2025. https://doi.org/10.3390/surfaces8030046
- [20] B. Shrisha, S. Bhat, D. Kushavah, and K. G. Naik, "Hydrothermal growth and characterization of Al-doped ZnO nanorods," *Materials Today: Proceedings*, vol. 3, no. 6, pp. 1693-1701, 2016. https://doi.org/10.1016/j.matpr.2016.04.061
- [21] M. Podlogar *et al.*, "Growth of transparent and conductive polycrystalline (0001)-ZnO films on glass substrates under low-temperature hydrothermal conditions," *Advanced Functional Materials*, vol. 22, no. 15, pp. 3136-3145, 2012. https://doi.org/10.1002/adfm.201200214
- [22] S. Akir, A. Hamdi, A. Addad, Y. Coffinier, R. Boukherroub, and A. D. Omrani, "Facile synthesis of carbon-ZnO nanocomposite with enhanced visible light photocatalytic performance," *Applied Surface Science*, vol. 400, pp. 461-470, 2017. https://doi.org/10.1016/j.apsusc.2016.12.212
- T. Tian et al., "Synthesis of large size ZnO microrods by a simple way of thermal evaporation," Ceramics International, vol. 41, pp. S774–S778, 2015. https://doi.org/10.1016/j.ceramint.2015.03.136
- [24] W. A. S. W. Razali, A. Nadzri, J. M. Sani, and M. N. Harif, "High vacuum PVD technique for enhancing zno thin films: Optical and electrical characterization," *Scientific Research Journal*, vol. 21, no. 2, pp. 135-147, 2024. https://doi.org/10.24191/srj.v21i2.27243
- M. Wang et al., "Performance optimization of atomic layer deposited ZnO thin-film transistors by vacuum annealing," IEEE Electron Device Letters, vol. 42, no. 5, pp. 716-719, 2021. https://doi.org/10.1109/LED.2021.3068992
- O. Akoa et al., "Simultaneous effect of precursor sources and concentration on structural, morphological and optical properties of ZnO nanostructured thin films for photovoltaic applications," *International Journal of Renewable Energy Development*, vol. 14, no. 3, pp. 495-504, 2025. https://doi.org/10.61435/ijred.2025.61069
- E. Rajalekshmi and A. M. E. Raj, "Effect of substrate temperature on structural and morphological studies by spray pyrolysed ZnO thin films," *Solid State Communications*, vol. 338, p. 114479, 2021. https://doi.org/10.1016/j.ssc.2021.114479
- [28] K. Ravichandran, N. Jabena Begum, S. Snega, and B. Sakthivel, "Properties of sprayed aluminum-doped zinc oxide films—a review," *Materials and Manufacturing Processes*, vol. 31, no. 11, pp. 1411-1423, 2016. https://doi.org/10.1080/10426914.2014.930961
- [29] C. Falcony, M. A. Aguilar-Frutis, and M. García-Hipólito, "Spray pyrolysis technique; high-k dielectric films and luminescent materials: A review," *Micromachines*, vol. 9, no. 8, p. 414, 2018. https://doi.org/10.3390/mi9080414
- S. Bose et al., "Elaboration of high-transparency ZnO thin films by ultrasonic spray pyrolysis with fast growth rate," Superlattices and Microstructures, vol. 156, p. 106945, 2021. https://doi.org/10.1016/j.spmi.2021.106945
- [31] H. Q. AL-Arique, S. S. AL-Qadasy, N. M. Kaawash, S. Chishty, and K. A. Bogle, "Study the characterization of ZnO and AZO films prepared by spray pyrolysis and the effect of annealing temperature," *Optical Materials*, vol. 150, p. 115261, 2024. https://doi.org/10.1016/j.optmat.2024.115261

- A. Bedia, F. Z. Bedia, M. Aillerie, N. Maloufi, and B. Benyoucef, "Morphological and optical properties of ZnO thin films prepared by spray pyrolysis on glass substrates at various temperatures for integration in solar cell," *Energy Procedia*, vol. 74, pp. 529-538, 2015. https://doi.org/10.1016/j.egypro.2015.07.740
- B. Bettayeb, D. Belamri, S. Benhamida, Y. Benkrima, A. Benmenined, and A. Manseri, "Effect of temperature deposition on the properties of Zno thin films prepared by low-cost nebulizer spray pyrolysis method," *Nanotechnology Perceptions* vol. 6, pp. 183-192, 2024. https://doi.org/10.62441/nano-ntp.v20i6.15
- [34] A. Ouhaibi, N. Saoula, M. Ghamnia, M. A. Dahamni, and L. Guerbous, "Effect of deposition temperature on morphological, optical, and photocatalytic properties of ZnO thin films synthesized by ultrasonic spray pyrolysis method," Crystal Research and Technology, vol. 57, no. 8, p. 2100224, 2022. https://doi.org/10.1002/crat.202100224
- [35] H. Nezzari, R. Saidi, A. Taabouche, M. Messaoudi, and M. S. Aida, "Substrate temperature effect on structural and optical properties of ZNO thin films deposited by spray pyrolysis," *Defect and Diffusion Forum*, vol. 397, pp. 1-7, 2019. https://doi.org/10.4028/www.scientific.net/DDF.397.1
- [36] E. Kärber et al., "Photoluminescence of spray pyrolysis deposited ZnO nanorods," Nanoscale Research Letters, vol. 6, no. 1, p. 359, 2011. https://doi.org/10.1186/1556-276X-6-359
- [37] J. S. Eensalu, M. Krunks, I. Gromyko, A. Katerski, and A. Mere, "A comparative study on physical properties of Aldoped zinc oxide thin films deposited from zinc acetate and zinc acetylacetonate by spray pyrolysis," *Energetika*, vol. 63, no. 2, 2017. https://doi.org/10.6001/energetika.v63i2.3519
- [38] H. F. McMurdie *et al.*, "Standard X-ray diffraction powder patterns from the JCPDS research associateship," *Powder Diffraction*, vol. 1, no. 2, pp. 64-77, 1986. https://doi.org/10.1017/S0885715600011593
- [39] F. Zahedi, R. Dariani, and S. Rozati, "Effect of substrate temperature on the properties of ZnO thin films prepared by spray pyrolysis," *Materials Science in Semiconductor Processing*, vol. 16, no. 2, pp. 245-249, 2013. https://doi.org/10.1016/j.mssp.2012.11.005
- P. Singh, A. Kumar, and D. Kaur, "Growth and characterization of ZnO nanocrystalline thin films and nanopowder via low-cost ultrasonic spray pyrolysis," *Journal of Crystal Growth*, vol. 306, no. 2, pp. 303-310, 2007. https://doi.org/10.1016/j.jcrysgro.2007.05.023
- [41] Y. Morinaga, K. Sakuragi, N. Fujimura, and T. Ito, "Effect of Ce doping on the growth of ZnO thin films," *Journal of crystal Growth*, vol. 174, no. 1-4, pp. 691-695, 1997. https://doi.org/10.1016/S0022-0248(97)00045-6
- [42] R. Ayouchi, F. Martin, J. R. Barrado, M. Martos, J. Morales, and L. Sánchez, "Use of amorphous tin-oxide films obtained by spray pyrolysis as electrodes in lithium batteries," *Journal of Power Sources*, vol. 87, no. 1-2, pp. 106-111, 2000. https://doi.org/10.1016/S0378-7753(99)00435-8
- [43] I. B. Kherchachi, H. Saidi, A. Attaf, N. Attaf, R. Azizi, and M. Jlassi, "Influence of solution flow rate on the properties of SnS2 films prepared by ultrasonic spray," *Optik*, vol. 127, no. 8, pp. 4043-4046, 2016. https://doi.org/10.1016/j.ijleo.2016.01.120
- [44] M. Mahajan *et al.*, "Green synthesis of ZnO nanoparticles using Justicia adhatoda for photocatalytic degradation of malachite green and reduction of 4-nitrophenol," *RSC Advances*, vol. 15, no. 4, pp. 2958-2980, 2025. https://doi.org/10.1039/D4RA08632E
- [45] R. S. Gaikwad, S. B. Jagdale, P. B. Pol, K. C. Mohite, and B. N. Pawar, "Effect of concentration of precursor on intrinsic ZnO thin films by spray pyrolysis," *Asian Journal of Multidisciplinary Studies*, vol. 2, no. 5, p. 110, 2014.
- [46] H. P. Asha, N. B. Gummagol, P. S. Patil, and B. Rajendra, "Modification of structure, electrical, linear and third-order nonlinear optical properties of spray pyrolyzed tin oxide films by deposition temperature," *Superlattices and Microstructures*, vol. 155, p. 106920, 2021. https://doi.org/10.1016/j.spmi.2021.106920
- [47] L. M. Balcazar and M. d. l. L. Olvera Amador, "IGZO thin films deposited by ultrasonic spray pyrolysis: Effect of Zn precursor milling and In and Ga concentration," *Journal of Materials Science: Materials in Electronics*, vol. 35, no. 12, p. 829, 2024. https://doi.org/10.1007/s10854-024-12412-y
- [48] A. F. Abdulrahman, S. M. Ahmed, S. M. Hamad, and A. A. Barzinjy, "Effect of growth temperature on morphological, structural, and optical properties of ZnO nanorods using modified chemical bath deposition method," *Journal of Electronic Materials*, vol. 50, pp. 1482-1495, 2021. https://doi.org/10.1007/s11664-020-08705-7
- [49] F. I. Abbas and M. Sugiyama, "Solution-dependent electrostatic spray deposition (ESD) ZnO thin film growth processes," *Materials Science*, 2024. https://doi.org/10.48550/arXiv.2406.13313
- [50] M. Amroun, K. Salim, A. Kacha, and M. Khadraoui, "Effect of TM (TM= Sn, Mn, Al) doping on the physical properties of ZnO thin films grown by spray pyrolysis technique: A comparative study," *International Journal of Thin Film Science and Technology*, vol. 9, no. 1, pp. 7-19, 2020. https://doi.org/10.18576/ijtfst/090102
- [51] M. Raj, J and L. Amalraj, "Effect of precursor concentration on physical properties of nebulized spray deposited In2S3 thin films," *Journal of Asian Ceramic Societies*, vol. 4, no. 3, pp. 357-366, 2016. https://doi.org/10.1016/j.jascer.2016.07.002
- [52] B. Bulcha *et al.*, "Synthesis of zinc oxide nanoparticles by hydrothermal methods and spectroscopic investigation of ultraviolet radiation protective properties," *Journal of Nanomaterials*, vol. 2021, no. 1, p. 8617290, 2021. https://doi.org/10.1155/2021/8617290

- [53] R. Gopikrishnan et al., "Synthesis, characterization and biocompatibility studies of zinc oxide (ZnO) nanorods for biomedical application," Nano-Micro Letters, vol. 2, no. 1, pp. 31-36, 2010. https://doi.org/10.1007/BF03353614
- [54] N. A. Ibrahim, A. A. Nada, B. M. Eid, M. Al-Moghazy, A. G. Hassabo, and N. Y. Abou-Zeid, "Nano-structured metal oxides: synthesis, characterization and application for multifunctional cotton fabric," *Advances in Natural Sciences:* Nanoscience and Nanotechnology, vol. 9, no. 3, p. 035014, 2018. https://doi.org/10.1088/2043-6254/aadc2c
- D. Yu, S. Mu, L. Liu, and W. Wang, "Preparation of electroless silver plating on aramid fiber with good conductivity and adhesion strength," *Colloids and Surfaces A: Physicochemical and Engineering Aspects*, vol. 483, pp. 53-59, 2015. https://doi.org/10.1016/j.colsurfa.2015.07.021
- [56] G. M. Abdelghani, A. B. Ahmed, and A. B. Al-Zubaidi, "Synthesis, characterization, and the influence of energy of irradiation on optical properties of ZnO nanostructures," *Scientific Reports*, vol. 12, no. 1, p. 20016, 2022. https://doi.org/10.1038/s41598-022-24648-x